Scientific Research Publishing

Optics and Photonics Journal, 2024, 14, 75-90
https://www.scirp.org/journal/opj
ISSN Online: 2160-889X
ISSN Print: 2160-8881

Numerical Simulation of Super-Resolution Structured Illumination Microscopy (SIM) Using Heintzmann-Cremer Algorithm with Non-Continuous Spatial Frequency Support

Mesfin Woldeyohannes[1], William McCray[2,3], Weiguo Yang[2]

[1]Department of Chemistry and Physics, Western Carolina University, Cullowhee, USA
[2]School of Engineering and Technology, Western Carolina University, Cullowhee, USA
[3]Department of Physics, North Carolina State University, Raleigh, USA
Email: wyang@wcu.edu

How to cite this paper: Woldeyohannes, M., McCray, W. and Yang, W. (2024) Numerical Simulation of Super-Resolution Structured Illumination Microscopy (SIM) Using Heintzmann-Cremer Algorithm with Non-Continuous Spatial Frequency Support. *Optics and Photonics Journal*, **14**, 75-90.
https://doi.org/10.4236/opj.2024.145005

Received: April 20, 2024
Accepted: May 28, 2024
Published: May 31, 2024

Abstract

We report a comprehensive numerical study of super resolution (SR) structured illumination microscopy (SIM) utilizing the classic Heintzmann-Cremer SIM process and algorithm. In particular, we investigated the impact of the diffraction limit of the underlying imaging system on the optimal SIM grating frequency that can be used to obtain the highest SR enhancement with non-continuous spatial frequency support. Besides confirming the previous theoretical and experimental work that SR-SIM can achieve an enhancement close to 3 times the diffraction limit with grating pattern illuminations, we also observe and report a series of more subtle effects of SR-SIM with non-continuous spatial frequency support. Our simulations show that when the SIM grating frequency exceeds twice that of the diffraction limit, the higher SIM grating frequency can help achieve a higher SR enhancement for the underlying imaging systems whose diffraction limit is low, though this enhancement is obtained at the cost of losing resolution at some lower resolution targets. Our simulations also show that, for underlying imaging systems with high diffraction limits, however, SR-SIM grating frequencies above twice the diffraction limits tend to bring no significant extra enhancement. Furthermore, we observed that there exists a limit grating frequency above which the SR enhancement effect is lost, and the reconstructed images essentially have the same resolution as the one obtained directly from the underlying imaging system without using the SIM process.

Keywords

Structured Illumination Microscopy, Super Resolution Imaging, Spatial

Frequency Support, Diffraction Limit

1. Introduction

The wave nature of light has long been known to pose a diffraction limit called Abbe diffraction limit on the far field image resolution that can be achieved using optical microscopy [1]. However, in the recent decade, several super resolution (SR) techniques have been proposed and demonstrated to enhance microscopic resolution beyond the diffraction limit, the main ones being stimulated emission depletion microscopy (STED), single-molecule localization microscopy (SMLM) including photoactivated localization microscopy (PALM) and stochastic optical reconstruction microscopy (STORM), as well as structured illumination microscopy (SIM) [1]-[8]. Of these optical super resolution techniques, the most widely adopted is the super resolution structured illumination microscopy (SR-SIM) technique due to its wide field-of-view, its ease of applicability to samples prepared for standard fluorescence microscopy, its multicolor imaging capability of up to four different color channels, and its relatively fast imaging speed and low intensity required for the optical excitation, making it the primary choice of super resolution for a wide variety of biological imaging problems such as imaging of living cells [9]-[12]. More recently, SR-SIM has been extensively experimented and extended to 3D optical sectioning SR-SIM, multi-color SR-SIM, plasmonic and localized plasmonic SR-SIM, and single-shot SR-SIM [10] [13]-[23]. Newly developed SR-SIM methods utilizing new reconstruction algorithms such as blind SIM and other machine learning based algorithms [23]-[28] are demonstrated to yield up to 14-fold of resolution enhancement [23]. These demonstrated SR performance surpasses other traditional SR microscopy techniques mentioned above. However, despite the wide adoption and fast development of these new SR-SIM methods, multiple fundamental challenges remain for SR-SIM including practical limits for SR enhancement, phase error of SIM that may lead failure of SR image reconstruction, as well as artifacts and other nuance imaging degrading effects due to insufficient coverage of spatial frequency components.

Fundamentally, all SR-SIM methods utilize Fourier transform technique whereby high spatial frequencies of an object which are beyond the diffraction limit are frequency mixed with a known structured illumination pattern to create beat frequencies (called Moiré fringes or Moiré patterns) that are below the diffraction limit and, therefore, can be detected in the far field. The high spatial frequencies encoded in these fringe patterns are then decoded by deconvolution algorithms to reconstruct the super-resolved image. In theory, SR-SIM offers unlimited image resolution enhancement, provided that a sufficiently wide range of spatial frequency components are recovered. However, not all SR-SIM recover a continuous range of spatial frequency support, resulting in exceedingly high resolution enhancement in some cases, while introducing imaging degrading effects which

lower the resolution of lower spatial frequency targets. SR-SIM with non-continuous spatial frequency support therefore presents at the same time an exciting opportunity for efficient SR-SIM and the challenges to understand the limit of such unconventional potentials.

In traditional SR-SIM, the structured illumination patterns (which usually are direction and phase shift controlled sinusoidal grating patterns) are projected onto the samples using the same underlying optical (microscopic) imaging system. Such an arrangement naturally limits the highest spatial frequency of the structured illumination patterns to that of the diffraction limit of the underlying imaging system. As a result, multiple sub-images acquired by varying the direction and phase shift of the grating make it possible to recover a continuous spatial frequency support up to twice the diffraction limit of the underlying imaging system, yielding up to two-fold enhancement of the lateral image resolution over and above the diffraction limit of the underlying imaging system. Further enhancement of image resolution requires wider range of spatial frequency be recovered which, in turn, requires the structured illumination patterns be directly imposed onto the samples instead of being projected from the underlying optical imaging system. As an example, plasmonic structured illumination microscopy (P-SIM), which utilizes higher grating frequency made possible by surface plasmon interference, has been demonstrated to yield about three-fold resolution enhancement over and above the diffraction limit [18] [19]. Other super-resolution structured illumination patterns including bulk and localized plasmonic modes, surface evanescent and Bloch waves, as well as random super-resolution speckles have also been successfully demonstrated to enhance the SR-SIM [17] [24] [29]-[32]. In the case where a 14-fold imaging resolution enhancement is demonstrated, hyperbolic metamaterials are used to achieve a record high cutoff spatial frequency that is 12 times that of the spatial frequency of the 488 nm light used, in addition to using up to 200 sub-images to reconstruct the SR image [23]. Though these new SR-SIM methods yield high resolution enhancement, the reconstructed images may still miss information over a large range or ranges of spatial frequencies due to the inherently non-continuous spatial frequency support of the methods.

In this paper, we present a comprehensive numerical simulation study that investigates the fundamental effects of SR-SIM grating frequency as related to the underlying diffraction limit, focusing in particular on the advantages as well as potential artifacts and image degradation effects due to the non-continuous spatial frequency support of the SR-SIM. Our results shine light on the attainable limits of resolution enhancement for SR-SIM methods that may utilize grating frequencies higher than the diffraction limit of the underlying optical imaging system. We also analyze simulation results showing the different side effects of such high SIM grating frequencies that, to the authors' best knowledge, have not been widely discussed previously. The comprehensive numerical study reported here provides empirical understanding of these issues that have been so far received less attention in the SR-SIM literature.

2. SIM Theory and Effects of Non-Continuous Support

In an SR-SIM, the frequency spectrum of the super-resolved image is generated by convolving high spatial frequency components of the object to be imaged which are above the diffraction limit of the imaging system with the spatial frequency components of a structured illumination that are allowable by the diffraction limit of the imaging system. If $O\left(k_x,k_y\right)$ and $S\left(k_x,k_y\right)$ are, respectively, the complex spatial frequency spectrum of the object and the magnitude of the structured illumination, and $H\left(k_x,k_y\right)$ denotes the spatial frequency transfer function of the imaging system, where k_x and k_y are lateral spatial frequencies, the spatial frequency spectrum of the super-resolved image $T\left(k_x,k_y\right)$ is given by the product of $H\left(k_x,k_y\right)$ with the convolution of $O\left(k_x,k_y\right)$ with $S\left(k_x,k_y\right)$ as:

$$T\left(k_x,k_y\right)=H\left(k_x,k_y\right)\left[O\left(k_x,k_y\right)*S\left(k_x,k_y\right)\right] \tag{1}$$

The autocorrelation of the complex function $H\left(k_x,k_y\right)$ yields the optical transfer function (OTF) of the images system which, in turn, is defined as the Fourier transform of the point spread function (PSF) of the system. Therefore, the OTF of an imaging system and, in turn, the spatial frequency transfer function $H\left(k_x,k_y\right)$ of the system determines the diffraction limit of the system, acting as a low-pass filter in the spatial frequency space. Without convolution with $S\left(k_x,k_y\right)$, the components of $O\left(k_x,k_y\right)$ with k_x or k_y that are higher than the diffraction limit of the imaging system cannot pass through the imaging system and, therefore, are unobservable, resulting in an image whose resolution is limited by diffraction. Convolution with $S\left(k_x,k_y\right)$ encodes higher spatial frequency components of $O\left(k_x,k_y\right)$ in the form of lower (observable) spatial frequencies, part of which can be decoded by a deconvolution algorithm, enhancing the image resolution beyond the diffraction limit [7] [8] [10] [11] [33].

In the original SR-SIM of Heintzmann and Cremer [8] [33], the structured illumination $S\left(k_x,k_y\right)$ consists of phase-shifted sinusoidal grating patterns aligned at 0, 90, 180, and 270 degrees, whereas in the more widely adopted SR-SIM of Gustafsson [7], the grating patterns are aligned at 0, 120, 240 degrees. Compared to Gustafsson's SIM configuration, Heintzmann-Cremer's configuration at multiples of 90 degrees corresponds to intensity extremes of the sinusoidal grating patterns and, therefore, is less susceptible to phase error, which is crucial to SIM reconstruction. Convolution with $S\left(k_x,k_y\right)$ simply adds copies of the original object spectrum at different locations determined by the phase and the spatial frequency of the grating pattern, shifting the higher spatial frequency components the object spectrum around the spatial frequency of the sinusoidal grating pattern to the passband of the OTF.

The fixed low-pass band of the OTF of the imaging system implies, at least in theory, that the higher the grating frequency, the higher the spatial frequency components of the object spectrum that can be resolved. As a result, if one wishes to reconstruct the spatial frequency components of the object over a continuous

spatial frequency range, the grating frequency should be that of the diffraction limit imposed by the OTF of the imaging system, doubling the spatial frequency range of the object that can pass the OTF. In turn, this implies that traditional SR-SIM is limited to two-fold lateral image resolution enhancement over and above the diffraction limit. On the other hand, for example for P-SIM, the grating frequency used in SIM may be much higher than that of the diffraction limit of the underlying optical imaging system. In such a case, super-resolution beyond the diffraction limit can also be achieved without the need to recover the continuous range of spatial frequency components. This is due to the sharpening effect of a non-continuous spatial frequency support on the lateral point spread function (LPSF) of the imaging system. This sharpening effect is best illustrated in Figure 1 where a hypothetical spatial frequency transfer function $H(k)$ with a noncontinuous range of spatial frequency support yields an LPSF with the main center lobe that is narrower than that of diffraction limit provided by the base passband. The smallest features such a sharpened LPSF filters selects, and hence the image resolution, is inversely proportional to the highest spatial frequency $H(k)$ supports, implying that the image resolution enhancement can be increased beyond two-fold of that supported by the base passband.

Intriguingly, Figure 1 shows that, an LPSF resulting from non-continuous spatial frequency coverage exhibits, besides a narrower center lobe, sizable side lobes.

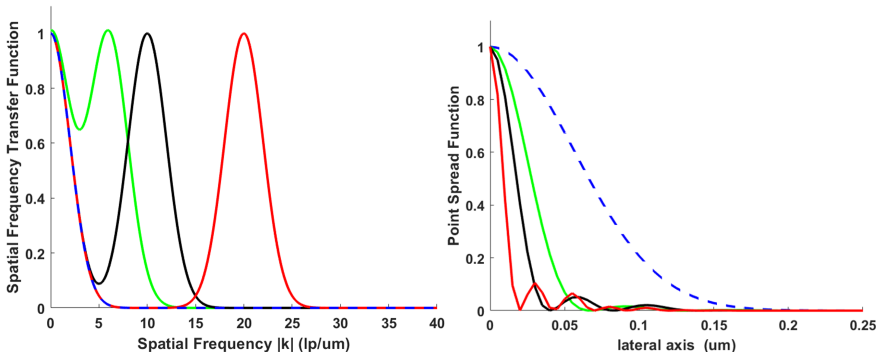

Figure 1. Super-resolution point spread functions (PSFs) from spatial frequency domain transfer function with noncontinuous range of spatial frequency support. Left: Spatial frequency transfer function; Right: the corresponding PSFs. The dashed PSF is the diffraction limit with the low-pass central support of spatial frequency only.

While much smaller in strength compared to the center lobe, which defines the smallest resolution, these non-monotonically decaying side lobes apparently are reasons for the difficulty in recovering the lower spatial frequency components of the object. The resulting images, while having the smallest resolvable features on par with the width of the center lobe of the LPSF, now have features at lower resolution "smeared". This "smearing", or loss of distinct features of lower spatial frequencies, is due to the convolution of lower spatial frequency components with the high spatial frequency components of the object in the SR-SIM process. If the

interference from the higher spatial frequency components of the object cannot be sufficiently removed, the SR-SIM employing grating frequencies higher than the diffraction limit of the underlying optical imaging system can resolve spatial frequencies of the object higher than the diffraction limit but may not resolve those on par with the diffraction limit. This side effect of SR-SIM employing high spatial frequency gratings such as in P-SIM is a peculiar feature that has not been given due attention in SR-SIM investigations. A concrete example of this effect is shown in the next section. Our simulations also show that there is a limit as to how high the grating frequency can be before losing all super-resolution enhancement and the reconstructed images from the SIM algorithm return to the same resolution limited by the underlying diffraction limit. Detailed discussions of these effects and their dependence on the grating frequency used are presented in the following sections.

3. Simulation Methods

In our numerical simulation, different aperture sizes are simulated by Gaussian shaped filters of different widths, the diffraction limit on the resolution of the underlying optical system being dependent on the width of the Gaussian filter. To quantify the dependence of the image resolution of the SR-SIM schemes on aperture size and grating frequency, we used a high-definition image of the standard 1951 USAF resolution test target (Figure 2(a)) for which the spatial frequency k in units of line pairs per millimeter (lp/mm) is given in terms of group and element numbers (n, m) by,

$$k = 2^{\left(n+\frac{m-1}{6}\right)} \tag{2}$$

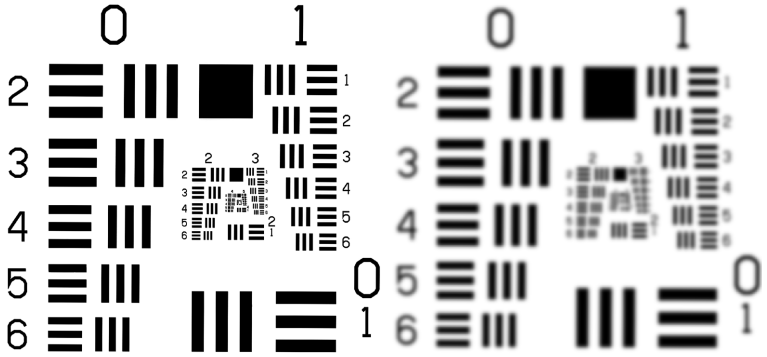

(a) (b)

Figure 2. (a) High definition image of the 1951 USAF resolution test target (Original JPEG picture file 2334 × 2334 pixels) used as the simulated object. (b) Simulated diffraction limited image obtained by passing the image target through a Gaussian spatial frequency domain filter.

For example, in Figure 2(b), the image target 2 - 3 (Group 2, Element 3) is the smallest target resolved (that is, the vertical and horizontal bars still recognizable as distinct bars and not blurred into one another) before the SR-SIM processes.

Therefore, the diffraction limit on the resolution of the underlying imaging system simulated by this Gaussian filter is $k = 2^{2+\frac{3-1}{6}} \approx 5.04$ lp/mm for $n = 2$ and $m = 3$. In comparison, the original JPEG picture (**Figure 2(a)**) has the highest resolved target 5 - 6, corresponding to $k_{max} = 2^{5+\frac{6-1}{6}} \approx 57$ lp/mm.

Figure 3 shows, for a given spatial frequency domain Gaussian blurring filter width in lp/mm, the spatial frequency of the smallest resolvable image target before the SR-SIM process. In other words, **Figure 3** plots the observed diffraction limit on the resolution of the simulated underlying imaging system as a function of the width of the spatial frequency domain Gaussian blurring filter. For example, for a filter width of 1.96 lp/mm, the diffraction limit is 2 lp/mm, whereas for a filter width of 11.44 lp/mm, the diffraction limit is about 11.31 lp/mm. As expected, larger the filter bandwidth, the smaller the target resolved, hence the higher the image resolution. As shown in the figure, the spatial frequency domain Gaussian filters have pretty good match over a large range of the simulated diffraction limits, from 1.5 lp/mm all the way to about 13 lp/mm.

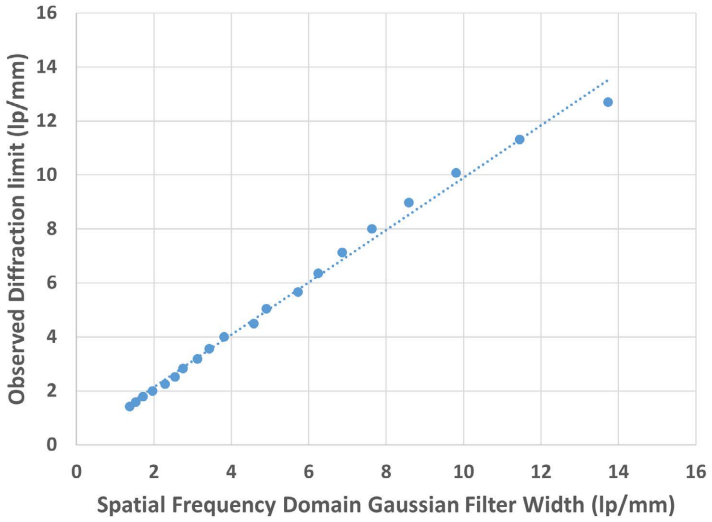

Figure 3. Observed simulated diffraction limits in lp/mm vs. the spatial frequency domain Gaussian filter used to simulate the diffraction effect. Spatial frequency of the smallest resolvable image targets vs. the blurring filter width before SR-SIM processing, simulating diffraction limits.

To investigate the dependence of the image resolution enhancement of the SR-SIM schemes on the grating frequency, we fix the width of the Gaussian blurring filter and impose sinusoidal illumination patterns of variable spatial frequencies onto the original image of the USAF resolution test target. Each resulting image is then reconstructed according to the Heintzmann-Cremer SR-SIM algorithm [7] [10] outlined in **Table 1**. The image quality for each grating frequency is determined by reading the group and element number of the smallest resolved target for that frequency. This process is illustrated in **Figure 4** which also an example of both the super-resolution effect and the side effects of non-continuous spatial

frequency support in the SR-SIM scheme discussed in the previous section.

Table 1. Heintzmann-Cremer SR-SIM algorithm.

Require:	Object **O**, optical imaging system **T**, phase adjustable linear sinusoidal grating of frequency **f**, SIM mixing parameter **alpha** (default to 0.1)
Output:	Reconstructed image **IR**.
Step 1:	Obtain the image **I** of the object
Step 2:	Align the linear grating in x direction, obtain four structure illuminated images, **I0**, **I90**, **I180**, and **I270** with grating imposed on the object with phase shifts of 0, 90, 180, and 270 degrees respectively
Step 3:	Let **A = I0 − I180**, **B = I90 − I270**
Step 4:	Let **Cx = (A − iB)*exp(−ifx)**, **Dx = (A + iB)*exp(ifx)**
Step 5:	Align the linear grating in y direction, repeat Step 2 to 4 to obtain **Cy** and **Dy**
Step 6:	Let the reconstructed image **IR = I + alpha*(Cx + Dx + Cy + Dy)**

In Figure 4, the effect of the OTF diffraction limit of the optical image system is simulated by a Gaussian filter of width of 11 pixels, corresponding to a spatial frequency width of 6.24 lp/mm. Figure 4(a) shows the image formed by the simulated underlying optical imaging system. Figure 4(a1) and Figure 4(a2) are close-ups of the increasingly smaller center regions to show the imaging resolution as a baseline comparison to the SR-SIM schemes simulated. The smallest target resolved by this base system is seen to be Group 2 Element 5 which corresponds to the spatial frequency of 6.35 lp/mm, consistent with the diffraction limit of the simulated optical imaging system. Figure 4(b) and Figure 4(c) show the recovered super-resolution images using SR-SIM with a grating frequency of 9.10 lp/mm and 14.56 lp/mm, respectively. Figure 4(b1) and Figure 4(b2), as well as Figure 4(c1) and Figure 4(c2), show the close-ups of the same smaller center regions as in Figure 4(a1) and Figure 4(a2). The grating frequencies used in Figure 4(b) and Figure 4(c) are 1.43 and 2.29 times of that of the diffraction limit simulated. Figure 4(b1) and Figure 4(b2) show a continuous range of image resolution enhancement up to Group 3 Element 6 which corresponds to a spatial frequency limit of 14.25 lp/mm, equating to a factor of 2.24 beyond the simulated diffraction limit. When the grating frequency is increased further as in the case of Figure 4(c), Figure 4(c2) shows that the smallest targets resolved are now in Group 4 ranging from Element 1 to 3, with the highest spatial frequency of 20.16, which is 3.17 times the underlying diffraction limit. However, for this high spatial frequency grating of 14.56 lp/mm (2.29 times the diffraction limit) and the super-resolution enhancement factor of 3.17 for the smallest distinguishable targets, some of the lower resolution targets like Group 3 Element 1, 2, and 3 become blurred, even though those targets that are resolved by the original underlying imaging system (Group 2 Element 5 and larger) still remain resolved, as can be seen from Figure 4(c1). In addition, for this particular example, all the super-

resolution enhancement effects are lost once the grating frequency is higher than 23.66 lp/mm or 3.73 times the underlying diffraction limit. These effects in general follow the same trend over all underlying diffraction limits and various grating frequencies simulated. Results of these comprehensive simulations are presented in the next section.

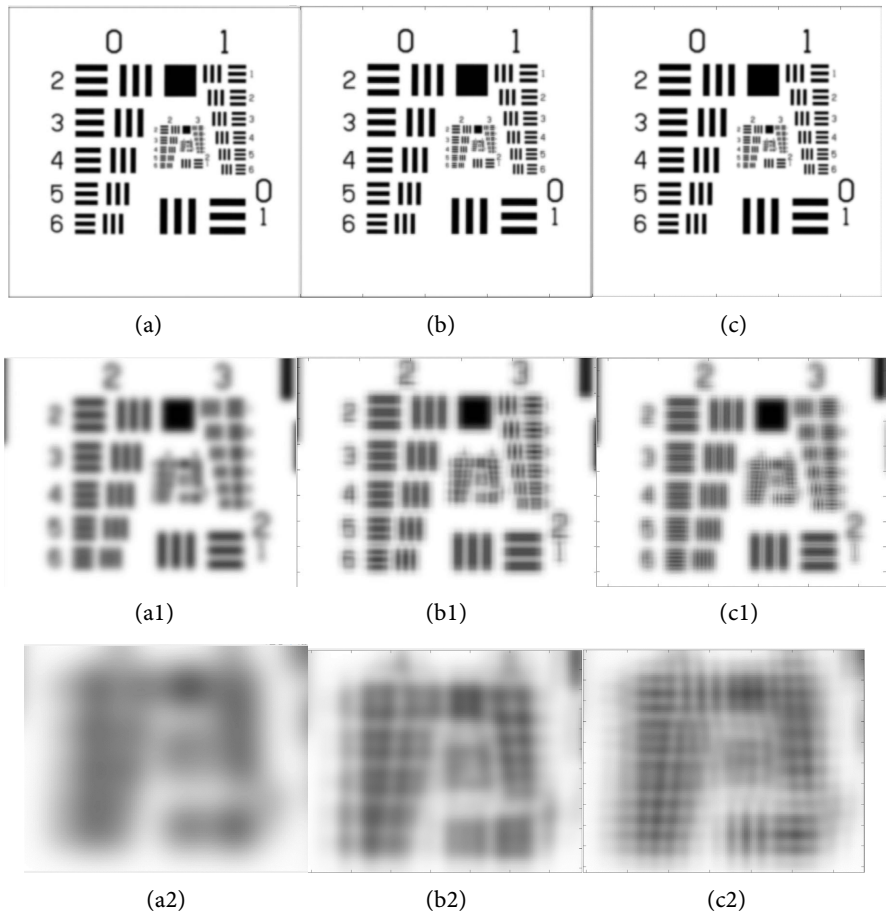

Figure 4. Super-resolution SIM images with low (b) and high (c) grating spatial frequencies are compared with the diffraction limited image from the simulated underlying optical imaging system. (a1) and (a2), and similarly (b1) and (b2), and (c1) and (c2) are the center regions of the same image of (a), (b), and (c), respectively, with increasing smaller imaging targets. This example shows that while the continuous spatial frequency support of SR-SIM such that as used in (b) results in a super-resolution enhancement factor of about 2, the higher grating spatial frequency, resulting in a non-continuous spatial frequency support like in most P-SIM cases such as used in (c), can result in a super-resolution enhancement factor of over 3 for the smallest targets resolved but may fail to resolve some of the lower spatial frequency targets as shown in (c1) and (c2).

4. Super-Resolution Effects over Various Underlying Diffraction Limits and Grating Frequencies

Figure 5 depicts the spatial frequency of the smallest resolvable image target for different SR-SIM grating frequencies, and for a spatial frequency domain Gaussian filter width fixed at 13.73 lp/mm for which the diffraction limit is 12.70 lp/mm,

as shown in Figure 3. From Figure 5 we see that, for a filter of width 13.73 lp/mm, SR-SIM grating frequencies higher than 5 lp/mm achieve image resolution beyond the diffraction limit (dashed line in Figure 5). Also apparent in the figure is the almost linear relationship between the highest spatial frequency of the resolved image target with the SR-SIM grating frequency, indicating that increase in SIM grating frequency directly translates into increase in the spatial frequency of the smallest feature resolved. This figure also shows that the SR-SIM process can indeed achieve image resolution beyond two times the diffraction limit. For example, for a grating frequency of 16.38 lp/mm, the spatial frequency of the smallest resolvable image is 25.40 lp/mm which is twice of the diffraction limit predicated in [9] [10]. For a grating frequency of 25.48 lp/mm, the smallest feature resolved has a spatial frequency of 35.92, which is 2.83 times the diffraction limit.

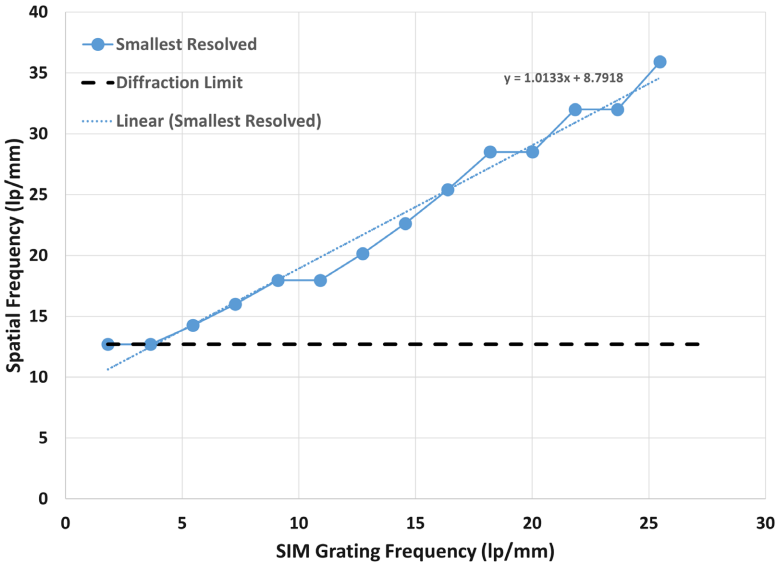

Figure 5. The solid Line shows spatial frequency of the smallest resolvable image targets vs. grating frequency after SR-SIM processing for a given Gaussian blurring filter width of 13.73 lp/mm. The diffraction limit for this case is about 12.70 lp/mm shown as the dashed line. The highest achieved super resolution enhancement is 2.83 times of the diffraction limit.

The proportional increase of SR enhancement does not extend indefinitely with increase in grating frequency. In fact, a grating frequency much higher than the diffraction limit of the underlying system can result in a total loss of the SR effect of the SIM. In addition, continuously resolved SR enhancement happens only for a moderate grating frequency range. Beyond this range, while the smallest resolvable targets can further improve in resolution, some of the lower resolution targets become blurred as discussed in previous section. When the grating frequency is increased further and exceeds certain limits, the entire SR effect disappears, and the recovered images largely return to the same resolution of the underlying system alone without using SIM. This is evident in Figure 6, which shows two underlying systems simulated with different spatial frequency domain Gaussian filters.

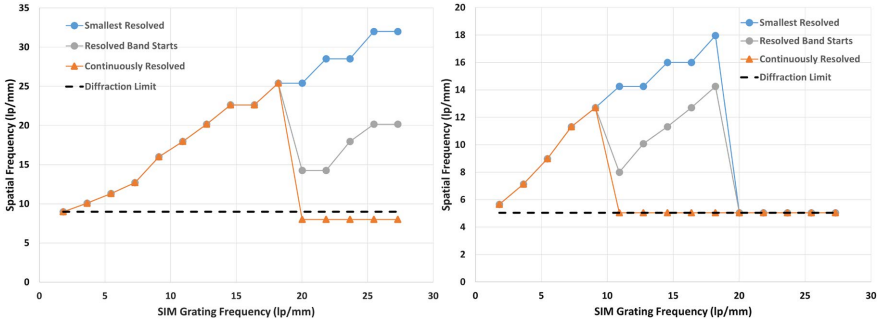

(a) (b)

Figure 6. Smallest resolved image target groups and the last resolved image target group before unresolved groups and their dependence on the grating frequency. (a) for filter width of 8.58 lp/mm for which diffraction limit of 8.98 lp/mm, and (b) for filter width of 4.90 lp/mm for which the diffraction limit of 5.04 lp/mm.

In **Figure 6(a)** and **Figure 6(b)** the spatial frequency domain Gaussian filter widths used to simulate the underlying imaging system are 8.58 lp/mm and 4.90 lp/mm respectively, for which the observed diffraction limits are 8.98 lp/mm and 5.04 lp/mm, respectively. As can be seen from the figures, the highest resolutions achieved using the simulated SR-SIM process by increasing the SIM grating frequency are 32.0 lp/mm and 17.96 lp/mm, both of which are about 3.56 times their respective diffraction limits. These highest resolution enhancements are achieved at the SIM grating frequencies of 25.48 lp/mm and 18.20 lp/mm, respectively, which are 2.84 and 3.61 times their respective diffraction limits. The continuously resolved highest resolutions, on the other hand, are 25.40 lp/mm and 12.70 lp/mm, respectively, which are 2.83 and 2.52 times their respective diffraction limits. These are achieved at SIM grating frequencies of 18.18 lp/mm and 9.10 lp/mm, respectively, which are 2.02 and 1.81 times their respective diffraction limits. Moreover, **Figure 6(a)** also shows that the continuously resolved smallest feature of the recovered image is at a slightly less resolution than that of underlying system alone without using SIM but the difference is nonetheless small. Finally, **Figure 6(b)** also shows that, beyond a certain limit for the SIM grating frequency which in this case is 20 lp/mm (~4 times of the diffraction limit), one loses all the SR effect and the SIM recovered images have the same resolution as the underlying imaging system alone without using the SIM process.

Figure 7 shows the highest SR enhancement factors achieved for both continuous and non-continuous enhancements of underlying imaging systems of different diffraction limits. The results depicted in the figure indicate that non-continuous enhancement utilizing the SIM grating frequency which is more than twice the diffraction limit of the underlying imaging system is most effective in obtaining the highest super-resolution enhancement relative to noncontinuous spatial frequency support. This extra enhancement scheme seems to lose its advantage over using moderate SIM grating frequencies that maintain continuous spatial frequency support as the diffraction limit of the underlying imaging system gets higher. In fact, as shown in the figure, when the diffraction limit of the underlying

imaging system is above 11 lp/mm, the two traces converge.

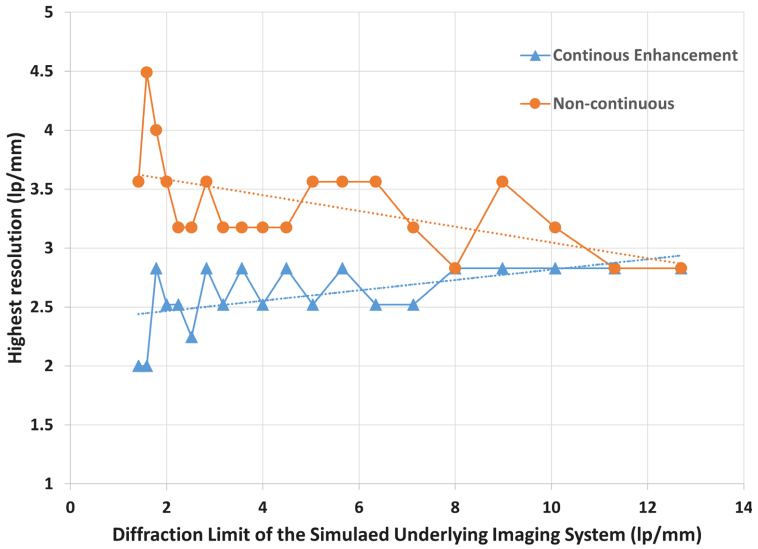

Figure 7. Highest super-resolution enhancement factors dependence on the diffraction limit of the simulated underlying imaging system. Triangle: Highest enhancement factor of continuous enhancement; Circle: Highest enhancement factor of non-continuous enhancement.

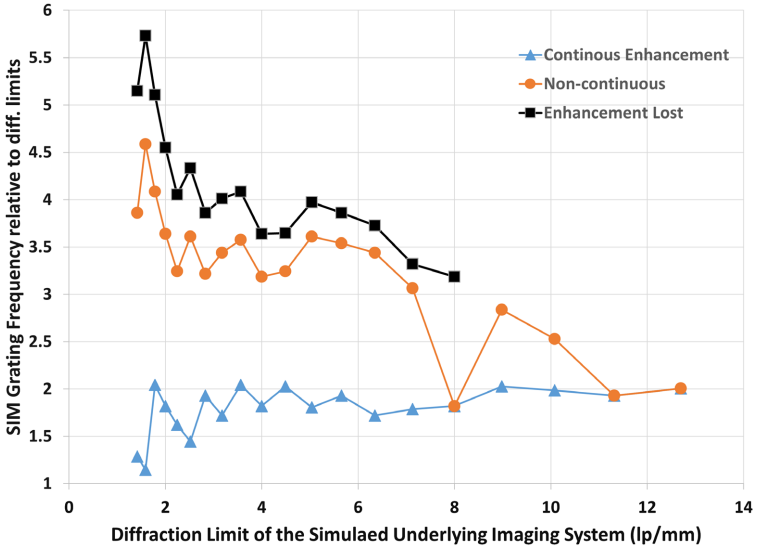

Figure 8. Optimal SIM grating frequencies for super-resolution enhancement v. s. the diffraction limit of the underlying imaging system. Triangles: Continuous spatial frequency support. Circles: Non-continuous spatial frequency support. Squares: the SIM grating frequency at and above which one loses the super-resolution effect.

Figure 8 shows the SIM grating frequencies at which the highest SR enhancement factors are obtained for both continuous and non-continuous enhancements, as well as the limit beyond which one loses all SR enhancement. As can be seen from the figure, for the conventional, continuous spatial frequency support, the optimal SIM grating frequencies (triangle trace in Figure 8) should be about

2 times the diffraction limits of the underlying imaging systems. From this result and Figure 7, it follows that the SR enhancement factor obtainable is about 2.5 to less than 3. On the other hand, for the smallest resolvable feature possible, and therefore, for the highest SR enhancement factors, one can utilize SIM gratings with grating frequencies that are as high as 4.5 times the diffraction limit of the underlying imaging system, which can yield a non-continuous spatial frequency support SR enhancement factor as high as 4.5. However, our simulation results seem to suggest that such non-continuous spatial frequency support schemes work well only when the diffraction limit of the underlying imaging system is low. For imaging systems starting with high diffraction limits, SIM grating frequencies above twice the diffraction limits do not bring significant extra resolution enhancement. Finally, when the SIM grating frequencies exceed certain limits (square trace in Figure 8), the SIM loses all the super-resolution effect, and the reconstructed images are of the same resolution as the underlying imaging system alone without SIM. Depending on the diffraction limits of the underlying imaging system, this SIM grating frequency limits seems to be in the range of 3 to 6.

5. Conclusions and Discussions

In conclusion, besides confirming the prediction that the original Heintzmann and Cremer's SR-SIM method can achieve image resolution enhancement close to 3 times the diffraction limit, our numerical simulation results have demonstrated a series of more subtle effects of the SR-SIM. We have shown that when the SIM grating frequency exceeds twice the diffraction limit, for underlying imaging systems whose diffraction limit is low, higher SIM grating frequencies can help achieve higher SR enhancement but do so at the cost of losing resolution at some intermediate spatial frequencies. When the underlying imaging systems start with high diffraction limits, SIM grating frequencies above twice the diffraction limits tend to bring no significant extra enhancement compared to the ones that are about twice the diffraction limit. This dependence on the initial diffraction limit of the underlying imaging system has not been widely reported. Furthermore, we found that there exists a limit grating frequency above which the SR enhancement effect is totally lost, and the reconstructed images essentially have the same resolution as those obtained directly from the underlying imaging system alone without using the SIM process. This is consistent with the literature where one observes that a super resolution image with N-fold resolution enhancement would require at least N^2 sub-images [24]. Since the Heintzmann-Cremer method uses 9 sub-images, when the grating frequency exceeds the limiting grating frequency, which closely follows the highest achievable resolution enhancement of ~3, the number of sub-images would not support the higher resolution enhancement. The comprehensive numerical simulations of Heintzmann and Cremer method SR-SIM presented here have demonstrated the advantages and limitations of the SR-SIM with non-continuous spatial frequency support. The conclusions reached here are expected to be applicable to other SR-SIM methods

including the Gustafsson method, which are more widely adopted in the field.

Acknowledgements

W. McCray was an undergraduate student at Western Carolina University during this research and is thankful to the support by National Science Foundation undergraduate student scholarship.

Conflicts of Interest

The authors declare no conflicts of interest regarding the publication of this paper.

References

[1] Kner, P., Manley, S., Shechtman, Y. and Stallinga, S. (2020) 25th Anniversary of STED Microscopy and the 20th Anniversary of SIM: Feature Introduction. *Biomedical Optics Express*, **11**, 1707-1711. https://doi.org/10.1364/boe.391490

[2] Betzig, E., Patterson, G.H., Sougrat, R., Lindwasser, O.W., Olenych, S., Bonifacino, J.S., *et al.* (2006) Imaging Intracellular Fluorescent Proteins at Nanometer Resolution. *Science*, **313**, 1642-1645. https://doi.org/10.1126/science.1127344

[3] Hess, S.T., Girirajan, T.P.K. and Mason, M.D. (2006) Ultra-High Resolution Imaging by Fluorescence Photoactivation Localization Microscopy. *Biophysical Journal*, **91**, 4258-4272. https://doi.org/10.1529/biophysj.106.091116

[4] Rust, M.J., Bates, M. and Zhuang, X. (2006) Sub-Diffraction-Limit Imaging by Stochastic Optical Reconstruction Microscopy (Storm). *Nature Methods*, **3**, 793-796. https://doi.org/10.1038/nmeth929

[5] Hell, S.W. and Wichmann, J. (1994) Breaking the Diffraction Resolution Limit by Stimulated Emission: Stimulated-Emission-Depletion Fluorescence Microscopy. *Optics Letters*, **19**, 780-782. https://doi.org/10.1364/ol.19.000780

[6] Klar, T.A. and Hell, S.W. (1999) Subdiffraction Resolution in Far-Field Fluorescence Microscopy. *Optics Letters*, **24**, 954-956. https://doi.org/10.1364/ol.24.000954

[7] Gustafsson, M.G.L. (2000) Surpassing the Lateral Resolution Limit by a Factor of Two Using Structured Illumination Microscopy. *Journal of Microscopy*, **198**, 82-87. https://doi.org/10.1046/j.1365-2818.2000.00710.x

[8] Heintzmann, R. and Cremer, C.G. (1999) Laterally Modulated Excitation Microscopy: Improvement of Resolution by Using a Diffraction Grating. *SPIE Proceedings*, **3568**, 185-196. https://doi.org/10.1117/12.336833

[9] Allen, J.R., Ross, S.T. and Davidson, M.W. (2013) Single Molecule Localization Microscopy for Superresolution. *Journal of Optics*, **15**, Article ID: 094001. https://doi.org/10.1088/2040-8978/15/9/094001

[10] Samanta, K. and Joseph, J. (2021) An Overview of Structured Illumination Microscopy: Recent Advances and Perspectives. *Journal of Optics*, **23**, Article ID: 123002. https://doi.org/10.1088/2040-8986/ac3675

[11] Ma, Y., *et al.* (2021) Recent Advances in Structured Illumination Microscopy. *JPhys Photonics*, **3**, Article ID: 24009.

[12] Zheng, X., Zhou, J., Wang, L., Wang, M., Wu, W., Chen, J., *et al.* (2021) Current Challenges and Solutions of Super-Resolution Structured Illumination Microscopy. *APL Photonics*, **6**, Article ID: 020901. https://doi.org/10.1063/5.0038065

[13] Schermelleh, L., Carlton, P.M., Haase, S., Shao, L., Winoto, L., Kner, P., *et al.* (2008)

Subdiffraction Multicolor Imaging of the Nuclear Periphery with 3D Structured Illumination Microscopy. *Science*, **320**, 1332-1336. https://doi.org/10.1126/science.1156947

[14] Qiao, C., Chen, X., Zhang, S., Li, D., Guo, Y., Dai, Q., *et al.* (2021) 3D Structured Illumination Microscopy via Channel Attention Generative Adversarial Network. *IEEE Journal of Selected Topics in Quantum Electronics*, **27**, 1-11. https://doi.org/10.1109/jstqe.2021.3060762

[15] Bajor, A.A. (2023) 3D Multi-Focus Structured Illumination Microscopy (MF-SIM) and Multi-Color SIM. Ph.D. Thesis, University of California. https://www.proquest.com/docview/2864837446

[16] Wang, M., Chen, J., Wu, W., Wang, L., Zheng, X., Xu, G., *et al.* (2023) Multi-Color Two-Photon Scanning Structured Illumination Microscopy Imaging of Live Cells. *Journal of BioPhotonics*, **16**, e202300077. https://doi.org/10.1002/jbio.202300077

[17] Bezryadina, A., Zhao, J., Xia, Y., Lee, Y.U., Zhang, X. and Liu, Z. (2019) Localized Plasmonic Structured Illumination Microscopy with Gaps in Spatial Frequencies. *Optics Letters*, **44**, 2915-2918. https://doi.org/10.1364/ol.44.002915

[18] Wei, F. and Liu, Z. (2010) Plasmonic Structured Illumination Microscopy. *Nano Letters*, **10**, 2531-2536. https://doi.org/10.1021/nl1011068

[19] Wei, F., Lu, D., Shen, H., Wan, W., Ponsetto, J.L., Huang, E., *et al.* (2014) Wide Field Super-Resolution Surface Imaging through Plasmonic Structured Illumination Microscopy. *Nano Letters*, **14**, 4634-4639. https://doi.org/10.1021/nl501695c

[20] Fernández-Domínguez, A.I., Liu, Z. and Pendry, J.B. (2015) Coherent Four-Fold Super-Resolution Imaging with Composite Photonic-Plasmonic Structured Illumination. *ACS Photonics*, **2**, 341-348. https://doi.org/10.1021/ph500342g

[21] Ponsetto, J.L., Bezryadina, A., Wei, F., Onishi, K., Shen, H., Huang, E., *et al.* (2017) Experimental Demonstration of Localized Plasmonic Structured Illumination Microscopy. *ACS Nano*, **11**, 5344-5350. https://doi.org/10.1021/acsnano.7b01158

[22] Lee, Y.U., Posner, C., Nie, Z., Zhao, J., Li, S., Bopp, S.E., *et al.* (2021) Organic Hyperbolic Material Assisted Illumination Nanoscopy. *Advanced Science*, **8**, Article ID: 2102230. https://doi.org/10.1002/advs.202102230

[23] Lee, Y.U., Nie, Z., Li, S., Lambert, C., Zhao, J., Yang, F., *et al.* (2022) Ultrathin Layered Hyperbolic Metamaterial-Assisted Illumination Nanoscopy. *Nano Letters*, **22**, 5916-5921. https://doi.org/10.1021/acs.nanolett.2c01932

[24] Lee, Y.U., Zhao, J., Ma, Q., Khorashad, L.K., Posner, C., Li, G., *et al.* (2021) Metamaterial Assisted Illumination Nanoscopy via Random Super-Resolution Speckles. *Nature Communications*, **12**, Article No. 1559. https://doi.org/10.1038/s41467-021-21835-8

[25] Shah, Z.H., Müller, M., Wang, T., Scheidig, P.M., Schneider, A., Schüttpelz, M., *et al.* (2021) Deep-Learning Based Denoising and Reconstruction of Super-Resolution Structured Illumination Microscopy Images. *Photonics Research*, **9**, B168-B181. https://doi.org/10.1364/prj.416437

[26] Zhang, Q., Chen, J., Li, J., Bo, E., Jiang, H., Lu, X., *et al.* (2022) Deep Learning-Based Single-Shot Structured Illumination Microscopy. *Optics and Lasers in Engineering*, **155**, Article ID: 107066. https://doi.org/10.1016/j.optlaseng.2022.107066

[27] Luo, F., Zeng, J., Shao, Z. and Zhang, C. (2023) Fast Structured Illumination Microscopy via Transfer Learning with Correcting. *Optics and Lasers in Engineering*, **162**, Article ID: 107432. https://doi.org/10.1016/j.optlaseng.2022.107432

[28] Chen, X., Zhong, S., Hou, Y., Cao, R., Wang, W., Li, D., *et al.* (2023) Superresolution Structured Illumination Microscopy Reconstruction Algorithms: A Review. *Light:*

Science & Applications, **12**, Article No. 172.
https://doi.org/10.1038/s41377-023-01204-4

[29] Li, Z., Kong, W., Wang, C., Pu, M., Luo, Y., Liu, X., *et al.* (2021) Waveguide Evanescent Waves Based Structured Illumination Microscopy with Compact Structure and Flexible Design. *Journal of Physics D*: *Applied Physics*, **54**, Article ID: 215101.
https://doi.org/10.1088/1361-6463/abe744

[30] Kong, W., Wang, C., Pu, M., Ma, X., Li, X. and Luo, X. (2021) Bloch Surface Wave Assisted Structured Illumination Microscopy for Sub-100 Nm Resolution. *IEEE Photonics Journal*, **13**, 1-9. https://doi.org/10.1109/jphot.2020.3044920

[31] Liu, X., Kong, W., Wang, C., Pu, M., Li, Z., Li, X., *et al.* (2021) Bulk Plasmon Polariton Based Structured Illumination Microscopy by Utilizing Hyperbolic Metamaterials. *Journal of Physics D*: *Applied Physics*, **54**, Article ID: 285103.
https://doi.org/10.1088/1361-6463/abf78b

[32] Mudry, E., Belkebir, K., Girard, J., Savatier, J., Le Moal, E., Nicoletti, C., *et al.* (2012) Structured Illumination Microscopy Using Unknown Speckle Patterns. *Nature Photonics*, **6**, 312-315. https://doi.org/10.1038/nphoton.2012.83

[33] Heintzmann, R. and Huser, T. (2017) Super-Resolution Structured Illumination Microscopy. *Chemical Reviews*, **117**, 13890-13908.
https://doi.org/10.1021/acs.chemrev.7b00218